Research Article

Chemical Review and Letters
journal homepage: www.chemrevlett.com
ISSN (online): 2645-4947 (print) 2676-7279

Computational study of metalloborophenes as an electronic sensor for the detection of the anticancer drug carmustine

Mercedeh Hemmatian[1], ShariehHosseini[2,] *, Hakimeh Ziyadi[1], Ehsan Shakerzadeh[3], Marjan Jebeli Javan[1]

[1]*Department of Organic Chemistry, TeMS.C., Islamic Azad University, Tehran, Iran.*
[2]*Department of Chemistry, TeMS.C., Islamic Azad University, Tehran, Iran.*
[3]*Chemistry Department, Faculty of science, Shahid Chamran University of Ahvaz, Ahvaz, Iran.*

ARTICLE INFO

Article history:
Received 07 August 2025
Received in revised form 06 November 2025
Accepted 24 November 2025

Keywords:
Carmustine
Biosensor
Fullerene
Surface adsorption
Density functional theory (DFT)

ABSTRACT

Recent studies have identified B_{40} fullerenes as promising candidates for biosensing applications, including the detection of medicinal agents, drug delivery, and gas nanosensing. In the present study, the adsorption behavior of carmustine on pristine B_{40} and metal-encapsulated fullerenes ($Mg@B_{40}$ and $K@B_{40}$) were investigated to evaluate their sensing capabilities using Density Functional Theory (DFT) calculations. The results revealed that the adsorption energies of carmustine on $M@B_{40}$ (M = Mg, K) were higher than pristine B_{40} fullerene, with the most stable conformer exhibiting an adsorption energy of –16.54 kJ/mol. Furthermore, the energy gap, defined as the difference between the highest occupied molecular orbital (HOMO) and the lowest unoccupied molecular orbital (LUMO), decreased upon carmustine adsorption, indicating an enhancement in enhanced electrical conductivity. Furthermore, Analysis of dipole moments and recovery times of the resulting complexes confirmed that these systems possess potential as Φ-type sensors for the selective detection of carmustine.

1. Introduction

Carmustine (Carm) is chemotherapeutic drug and an alkylating agent that is specifically used in the treatment of various cancers[1-4]. carmustine is used for treatments of beginning stage of brain tumors, myeloma and Hodgkin's lymphoma. Furthermore, it can be used in treatments of liver and digestion carcinomas and melanoma. carmustine as an intravenously administered drug that can cross the blood–brain barrier may be effective in treating brain tumors due to proposed alkylating the DNA mechanism [5-7]. This process helps in inhibiting enzymes, prevents amino acid binding, and disrupts protein synthesis, which ultimately leads to a halt in cancer cell proliferation. Its metabolism is by the liver, and it is excreted through the kidneys in general. Its side effects include reduction in white blood cells or inflammatory infection, pulmonary fibrosis, and reduction of blood's platelets. This drug can be administered along with other anticancer drugs to enhance its therapeutic efficiency [8-14].

Therefore, due to the significance of this drug, development of new techniques for its detection is essential. To date, various analytical techniques have been used for the detection of carmustine, such as the mass spectrometry, liquid chromatography, nuclear magnetic resonance (NMR) spectroscopy, and ultraviolet-visible (UV-Vis) spectroscopy [15-17]. However, these techniques have shortcomings such as high costs and low sensitivity. Despite numerous advancements in medicine, cancer remains one of the most lethal diseases, highlighting the crucial need for developing new treatment approaches with minimal adverse effects. Nanostructures and their derivatives are very important owing to their applications in magnetic recording imaging, electronic materials and devices, environmental processes, drug transport, etc [18-23].

Recently, nanomaterials such as nanosheets, nanochains, nanoclusters, and nanotubes have been utilized as new sensors because of their unique characteristics including their large surface-to-volume ratios and electronic sensitivity [24-28]. For example, gold nanoclusters exhibit fluorescence changes upon interaction with carmustine [29, 30]. In addition, metal-doped graphene such as molybdenum, gold, copper, and silver has been used as biosensors for carmustine's

* Corresponding author E-mail: shariehhosseini@yahoo.com
https://doi.org/10.22034/crl.2025.539949.1669

adsorption [31].

Fullerenes have been utilized as adsorbents for gas and pollutants and as biosensors for detection applications [32-37]. Among boron-based fullerenes, B_{40} stands out as the most stable structure due to its electron deficiency, thus having potential for strong interactions. It has both acidic and basic properties. Moreover, its conductivity can be enhanced by metal doping or encapsulation [38-44]. In 2020, Changyu Li et al. investigated the detection of sulfur-containing gases by boron fullerenes alone. Their findings demonstrated that B_{40} nanocluster could act as Φ-type gas sensors and serve as electronic sensors for detecting CS_2 and SO_2 gases [45]. In another study, Shakerzadeh et al. investigated pristine and lithium-encapsulated B_{40} fullerenes as chemical sensors for the detection of NO_2 pollutants using computational technique. Their findings demonstrate that these fullerenes may be employed as effective chemical sensors for pollutants [40]. Furthermore, fullerenes can also serve as biosensors for drugs detection, particularly for anticancer drugs [46-52].

In this project, the biosensing capabilities of pristine and encapsulated (M = Mg and K) B_{40} fullerenes are investigated for the detection of carmustine, an anticancer drug. The novelty lies in the first-time theoretical investigation of metalloborophene sheets as electronic sensors for detecting the anticancer drug carmustine using density functional theory (DFT). While previous studies have reported the sensing performance of pristine borophene or metalloborospherene materials toward other analytes such as metronidazole, cisplatin, and 5-fluorouracil , no computational or experimental report has explored the interaction between metalloborophenes and carmustine molecules[41, 42, 53].

This work introduces metal-doped borophene (M–B) systems as a new class of two-dimensional sensor materials, expanding the sensing capabilities of boron-based nanostructures to nitrosourea drugs. Through a comparative DFT analysis, the study reveals how transition metal doping modifies charge transfer, adsorption energy, and electronic conductivity, establishing metalloborophene as a promising, selective, and sensitive platform for carmustine detection. Such findings open new possibilities for designing multifunctional boride-based nanosensors for anticancer drug monitoring, which has not been previously reported in the literature.

2. Materials and Methods

The first and most fundamental step in the theoretical investigation of drug molecules and nanocarriers is the optimization of their geometric structures, which is essential for extracting key molecular properties such as adsorption energy, thermochemical parameters, charge distribution, energy gap, etc. The specific convergence criteria for geometry optimizations have now been clearly described to ensure computational reproducibility. In our calculations, convergence was achieved when the maximum force (GMAX) and root mean square (RMS) force (GRMS) were below $4.5\times10^{-4}$and 3.0×10^{-4} Hartree/Bohr, respectively, while the maximum and RMS displacements (XMAX and XRMS) were below 1.8×10^{-3} and 1.2×10^{-3} Å, respectively. These thresholds correspond to the default (tight) convergence criteria commonly employed in quantum chemical geometry optimizations, ensuring reliable equilibrium geometries.

Then, the molecular structures of carmustine, pristine B_{40} fullerene, and B_{40} fullerenes that were encapsulated with magnesium (Mg) and potassium (K) were first constructed using Gauss View 06 software[54]. Subsequently, geometrical optimization and frequency calculations were performed using Gaussian 09 software[55], using Density Functional Theory (DFT) with the B3LYP functional and the 6-31G* basis set[38, 56, 57] . The B3LYP functional, which merges Becke's three-parameter exchange with the Lee–Yang–Parr correlation components, offers an effective balance between accuracy and computational efficiency, making it widely applicable to both organic and organometallic systems. The selected 6-31G* basis set, a polarized double-ζ type, incorporates polarization functions that enhance the modeling of electron distribution and molecular geometries, thereby improving the reliability of optimized structures and orbital representations.

The B3LYP/6-31G* combination has been extensively validated for predicting molecular geometry, vibrational spectra, and electronic properties of small- and medium-sized molecules. This approach provides a robust compromise between computational cost and predictive accuracy, making it particularly suitable for exploring molecular adsorption, reactivity trends, and charge transfer phenomena. While this level of theory does not explicitly account for long-range dispersion interactions and may be subject to basis set superposition error (BSSE), previous benchmark studies demonstrate that internal error compensations render it a reliable and justified selection for preliminary DFT-based investigations.

To examine the electronic properties, electron conductivity, and electronic descriptors such as HOMO energy (E_{HUMO}), LUMO energy (E_{LUMO}), gap energy (E_g), energy of Fermi level (E_f), chemical potential (μ), and electrophilicity (ω), the following quantities were computed. The fullerenes adsorption energy of interaction was computed using equation (1).

$$Eads = EComplex - (Ecarmustineustine + EFullerene) \quad (1)$$

where E_{ads} is the fullerenes adsorption energy of interaction, $E_{Complex}$ is the energy of the drug-fullerene complex, $E_{carmustine}$ is carmustine's energy, and $E_{Fullerene}$ is the energy of the fullerenes.

Energy gap for all structures was determined via the

following equation:

$$Eg = ELUMO - EHOMO \quad (2)$$

where E_g is the energy gap, and the energies of the lowest unoccupied and highest occupied molecular orbitals are denoted by $E_{LUMO\ and}\ E_{HOMO}$, respectively. The electronic sensitivity of fullerenes toward the carmustine drug, is assessed by the percentage change of the E_g as follows:

$$\Delta Eg = [(Eg2 - Eg1)/Eg1] \times 100\% \quad (3)$$

Where E_{g1} and E_{g2} represent the energy gaps of the bare fullerene and the complex, respectively [43]. For drawing the density of state (DOS) diagrams, the MultiWFN program was utilized[58]. NBO analyses are efficient tools for representing electron density in numerous systems. NBO analyses were carried out at the B3LYP/6-31G(d) level. This approach quantifies donor–acceptor (bond–anti bond) interactions by evaluating their second-order perturbation stabilization energies (E2)[59-61]. These E2 values were calculated as follows:

$$E^2 = \Delta E_{ij} = q_i \frac{F(i.j)^2}{\varepsilon_j - \varepsilon_i} \quad (4)$$

where, F(i,j) is the off-diagonal part of the NBO Fock matrix, qi is the orbital occupation of the donor, and εi; εj are the diagonal components (orbital energies).

3. Results and Discussion

The optimized structure of carmustine drug and the fullerenes is shown in Figure 1. The bond length and the bond angles derived from the computation matches those obtained from previous experimental results[51]. Therefore, the basis set and the functional used were suitable for the studied complexes.

Several studies have shown that negatively charged solid adsorbents can exhibit specific adsorption capabilities. Moreover, it appears that metal-encapsulated fullerenes have stronger adsorption capabilities. studies conducted on fullerenes that have been encapsulated with different metals such as those from the alkaline earth, and transition metal groups indicate that the presence helps of metal promotes stronger interaction and causes electric conductivity to increase compared to a pristine fulleren [42].

This encapsulation not only improves the sensor capabilities and properties of fullerenes but also aids in the detection of drugs and gases. Mg and K were particularly suitable for B_{40} encapsulation compared to other metals because Both are biologically essential and non-toxic at therapeutic levels. Their ionic sizes and moderate reactivities are compatible with stable B_{40} encapsulation. They effectively tune the B_{40} nanocluster's electronic structure, improving adsorption energies and charge transfer characteristics critical for drug delivery performance.

Thus, encapsulating Mg and K within B_{40} not only enhances the nanocage's electronic reactivity and drug interaction potential but also ensures biocompatibility and safety for targeted drug delivery systems.

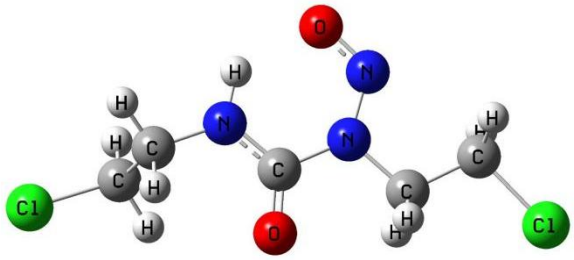

a. carmustine

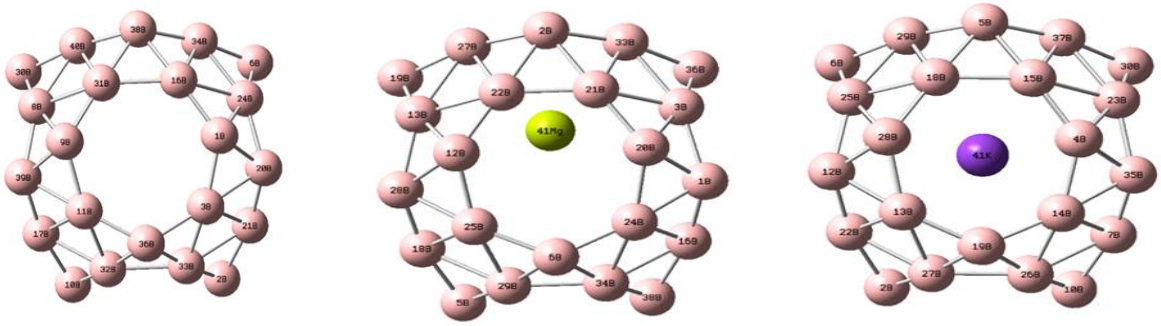

b. B40 **c.** Mg@B40 **D.** K@B40

Fig. 1. optimized structures of a) carmustine, b) B40, c) Mg@B40, d) K@B40

To find the most stable conformer, carmustine with various functional groups was brought close to the rings of a six or seven-sided fullerene from various directions (parallel or vertical) for binding.

The most stable conformers obtained were those interacting with the fullerene through two functional groups: chlorine and oxygen (Figure 2). Among these structures, the conformers interacting via the oxygen atom exhibited more negative adsorption energies. In the B40/carm complex, the second most stable conformer, in which carmustine approaches the fullerene through the chlorine atom, exhibits an adsorption energy of −9.98 kJ·mol^{-1}. This value indicates lower stability compared to conformer 1, which possesses an adsorption energy of −14.18 kJ·mol^{-1}. Furthermore, the chlorine–fullerene separation in conformer 2 is larger than the corresponding oxygen–fullerene distance observed in conformer 1. Although a shorter interaction distance does not necessarily imply greater stability, the adsorption energy values serve as the primary criterion for determining the relative stability of the conformers.

The results presented in Table 1 also indicate that the presence of magnesium and potassium metals inside the nanocage leads to the formation of more stable complexes with more negative binding energies.

The adsorption energy values reported in Table 1 suggest that the adsorption of the carmustine drug on fullerene occurs through physical adsorption, involving electrostatic and other non-covalent interactions.

Figure 3 depicts the adsorption energy values of all investigated complexes before and after metal encapsulation within the B_{40} fullerene.

Generally, conformer no. 1 structures display higher adsorption energies than their corresponding conformer no. 2 counterparts.

Within the conformer no. 1 series, the carm/Mg@B_{40} complex exhibits the most pronounced adsorption energy of –16.45 kJ/mol.

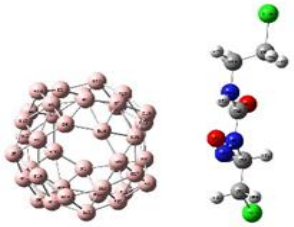

a. Carm/B40

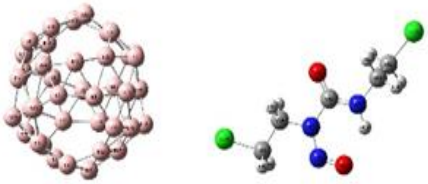

b.Carm/B40

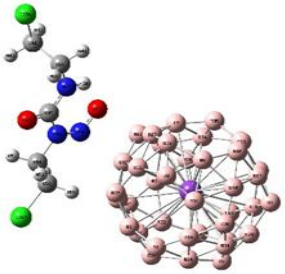

c. Carm/K@B40

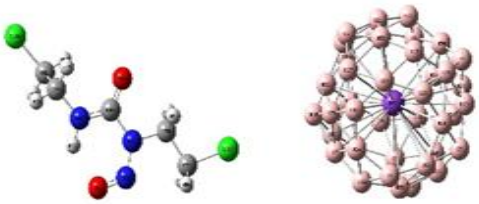

d. Carm/K@B40

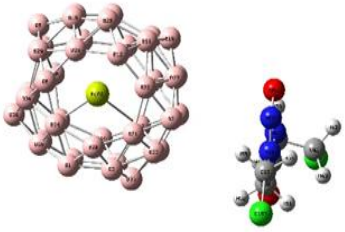

e.Carm/Mg@B40

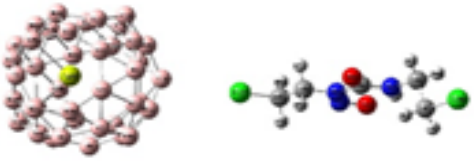

f. Carm/Mg@B40

Fig. 2. Optimized structures of carmustine (Carm) adsorbed onto a) and b) B40, c) and d) K@B40 and, e) and f) Mg@B40

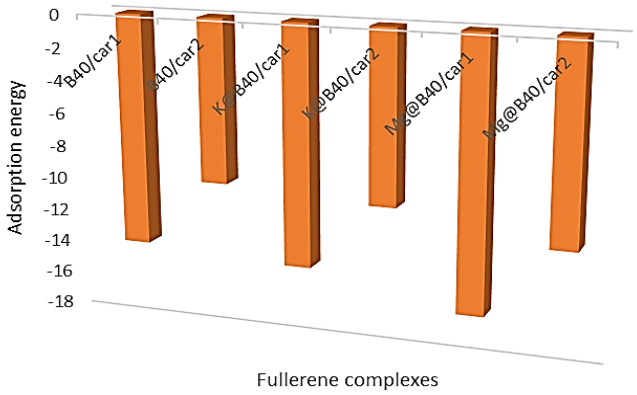

Fig. 3. Diagram of adsorption energies of B40 and M@B40 fullerene complexes (M=K and Mg)

The study of electric charge shows that a charge transfer from carmustine to encapsulated fullerene has taken place. This is primarily due to carmustine being a polarized molecule bearing electronegative atoms.

Fullerene does not possess significant dipole moment. However, placing a magnesium (Mg) or potassium (K) atom inside the nanocage, as shown in Table 1, leads to an increase in the dipole moment of fullerenes. Since dipole moment is a vector quantity, once carmustine is adsorbed, dipole moments align and increase in magnitude. The dipole moment is a suitable measure of the electric charge distribution pattern in each system. In principle, the greater the dipole moment, the more observable the solvent effect will be, and solubility in polar solvent such as water increases. Considering the data in Table 1, it can be concluded that once carmustine is adsorbed, the dipole moment increases considerably. This increase is nearly double in magnesium-encapsulated fullerene compared to pristine fullerene. Whereas in K@B40, the increase is negligible. This considerable increase in the case of magnesium (Mg) can be attributed to higher charge distribution, since a magnesium ion (Mg^{++}) has two positive charges, compared to one positive charge in a potassium ion (K^{+}).

A deeper understanding of the electronic modifications induced by the adsorption of carmustine on the pristine and metal-encapsulated fullerenes is provided through the total density of states (TDOS) diagrams presented in Figure 4.

The potential of fullerene as a molecular sensor for the detection of carmustine was subsequently investigated. To achieve this, two parameters-energy gap (E_g) and work function (Φ) were calculated. One of the key parameters in evaluating the sensitivity of a nanostructure is the energy gap, which correlates with electrical conductivity according to the following equation [62].

$$\text{Electrical Conductivity} = A\sqrt[3]{T}\,e^{\frac{-Eg}{2KT}} \quad (5)$$

where K is the Boltzmann's constant and A is a constant quantity. In this equation, energy gap has an inverse relationship with electrical conductivity.

In addition, the effect of carmustine drug on the Fermi level energy (E_f) and work function (Φ)-two of the key parameters in Φ-type sensors- was examined. The work function (Φ) is defined as the minimum energy required to remove an electron from the Fermi level to vacuum [63, 64].

A Kelvin oscillator instrument was utilized to measure the value of Φ before and after molecule adsorption in the Φ-type detectors.

Table 1. Dipole moment (Dm, Debye), adsorption energy (Eads, kJ/mol), energy of HOMO (E_{HOMO}, energy of LUMO (E_{LUMO}, eV), HOMO-LUMO energy gap (Eg, eV), energy of Fermi level (EF, eV)), work function (Φ), and recovery time (τ, s). The %ΔEg and %ΔΦ indicate the change of Eg and Φ after the adsorption process

Structure	Dm	E_{ads}	E_{HOMO}	E_{LUMO}	E_g	%ΔEg	E_F	Φ	%ΔΦ	τ
B40	0.004	-	-5.77	-2.83	2.94	-	-4.30	4.30	-	-
Mg@B40	0.3	-	-4.19	-2.73	1.45	-	-3.46	3.46	-	-
K@B40	0.00۲	-	-4.079	-2.81	1.26	-	-3.45	3.45	-	-
B40/Carm1	2.6	-14.18	-5.77	-2.83	2.93	-0.34	-4.301	4.301	0.000	3*10 -10
B40/Carm2	2.57	-9.98	-5.77	-2.83	2.93	-0.34	-4.299	4.299	-0.032	6*10 -11
Mg@B40/Carm1	4.67	-16.54	-4.19	-2.76	1.43	-1.38	-3.476	3.476	0.432	8*10 -10
Mg@B40/Carm2	4.64	-12.08	-4.17	-2.72	1.45	0	-3.448	3.448	-0.393	1.3* 10 -10
K@B40/Carm1	2.67	-14.7	-4.08	-2.83	1.25	-0.8	-3.459	3.459	0.355	4*10 -10
K@B40/Carm2	2.51	-10.5	-4.08	-2.82	1.26	0	-3.452	3.452	0.158	7*10 -11

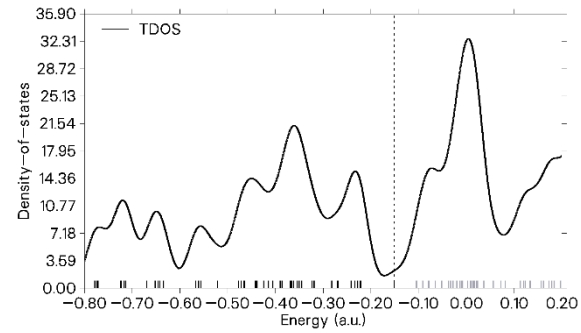

a1. K@B40

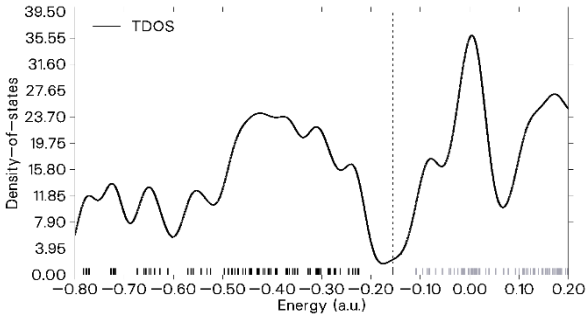

a2. Carm/K@B40

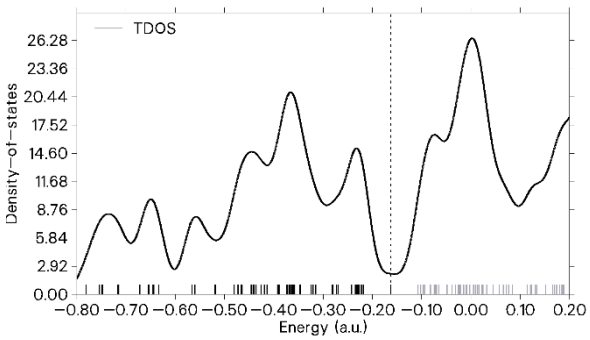

b1.Mg@B40

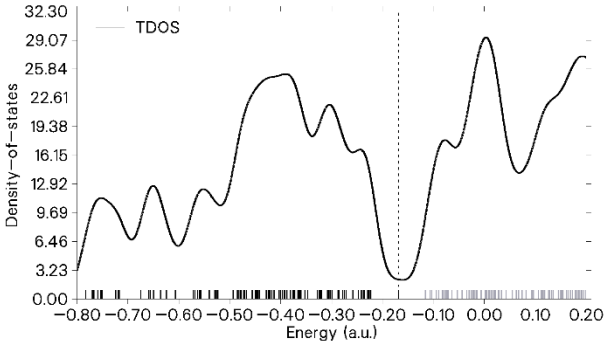

b2. Carm/Mg@B40

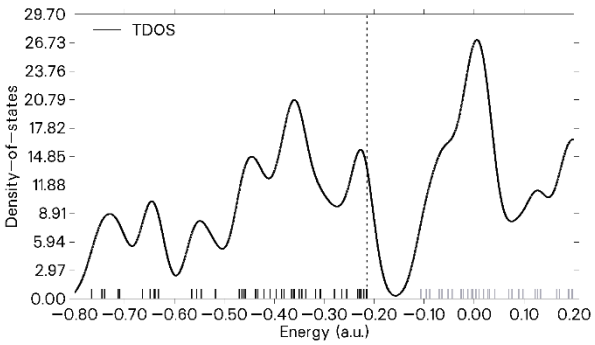

c1. B40

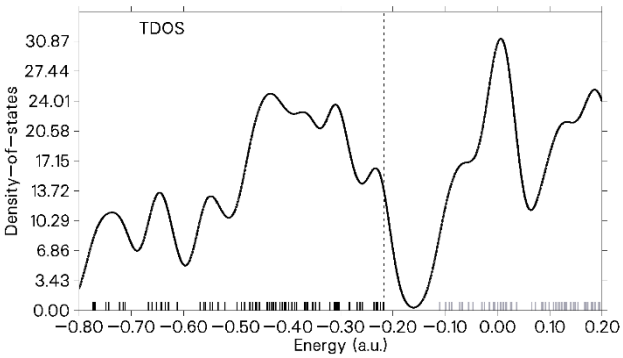

c2. Carm/B40

Fig. 4. Total density of states (TDOS) diagrams of a1) K@B40, a2) Carm/K@B40, b1) Mg@B40, b2) Carm/Mg@B40, c1) B40, c2) Carm/B40

When the adsorption of a molecule increases or decreases the work function of the sensor, it alters the gate voltage, thereby generating an electrical signal that facilitates chemical detection.

$$\Phi = Vel(+\infty) - EF \tag{6}$$

Here, E_F denotes the Fermi level energy, and Vel (+∞) represents the electrostatic potential energy of an electron far from the material's surface, which is assumed to be zero. Therefore, assuming Vel (+∞) = 0, the following expression can be written:

$$\Phi = -EF \tag{7}$$

The Fermi level energy is calculated using the following expression:

$$EF = E\,HOMO + \left(\frac{ELUMO - EHOMO}{2}\right) \tag{8}$$

Classical Richardson Dushman equation explains that the variation in the work function (Φ) of a sensor, due to changes in the Fermi level energy, can affect the amount of field emission (equation 8):

$$j = AT^2 e^{-\Phi/KT} \tag{8}$$

In this equation, $\boldsymbol{j}$ is the electron emission current density, A refers to the Richardson constant (A/m²), and

T represents the temperature in Kelvin (K) [65].

The change in the Φ upon carmustine adsorption is calculated as follows:

$$\%\Phi = (\Phi 2 - \Phi 1)/\Phi 1 \times 100 \quad (9)$$

In this context, Φ_1 and Φ_2 denote the values of Φ for the bare fullerene and the Carm/fullerene complex, respectively.

Based on the results presented in Table 1, no significant variations were observed in the HOMO–LUMO energy gap (Eg), Fermi level energy (EF), or work function (Φ) following the adsorption of carmustine on pristine B40 fullerene for conformer 1 (B40/Carm1). These parameters exhibited only negligible changes for conformer 2 (B40/Carm2). Therefore, pristine B40 cannot function as an effective Φ-type sensor. In contrast, substantial variations in both the energy gap and the work function were observed upon the adsorption of carmustine onto the Mg-encapsulated B40 fullerene. For the Carm/Mg@B40(1) conformer, the calculated changes in the energy gap and work function were -1.32% and 0.43%, respectively, suggesting that this system could serve as an efficient Φ-type molecular sensor for detecting the carmustine drug. As shown in Table 1, the energy gap (Eg) values for both B40/Carm1 and B40/Carm2 after adsorption are 2.93 eV, indicating an insignificant difference compared with the pristine B40 fullerene (2.94 eV). In contrast, the variations in the energy gap for the metal-encapsulated fullerenes are more pronounced. Among these systems, the lowest energy gap is observed when a potassium (K) atom is encapsulated within the nanocage (K@B40/Carm1), yielding a value of 1.25 eV. According to equation (4), this reduction in the energy gap corresponds to an enhancement in the electrical conductivity of the system. Electronic sensors operate based on the change in the electric conductivity upon molecular adsorption. This is because variations in conductivity can be converted into electric signals, thereby enabling the detection of the adsorbed drug. Based on the results obtained, fullerenes can act as effective electric sensors for detecting the carmustine drug.

According to Table1, the highest and lowest electrical conductivity among the studied complexes correspond to Carm/K@B40(1) and Carm/B40 fullerenes respectively. Therefore, the presence of alkali and earth alkali metals into the fullerene nanocage enhances its structural properties, leading to increased adsorption energy and improved electric conductivity.

The energy level of HOMO (E_{HOMO}) is significantly affected upon the adsorption of carmustine. A noticeable reduction in E_{HOMO} is observed for metal-encapsulated fullerenes compared to the bare fullerene. In contrast, the energy level of the lowest unoccupied molecular (E_{LUMO}) remains almost unchanged after adsorption

The TDOS diagrams in Figure 4 also confirm the emergence of a new electronic state following adsorption of carmustine.

Moreover, a noticeable shift in the HOMO level from the fullerene surface to the carmustine molecule, in line with the large change in HOMO energy.

The strength of interaction plays a critical role in sensor development, as strong interactions make the desorption process more difficult. According to the following equation, an increase in the adsorption energy leads to a longer recovery time for the interaction [64, 66]:

$$\tau = \frac{1}{\upsilon} exp(-Ea/KBT) \quad (10)$$

Where K_{BT} is the Boltzmann's constant (-2.0 x 10^{-3} kcal/mol.K), T is the temperature in Kelvin, and ν is the attempt frequency. As depicted in Table 1, the fullerene complexes under study, show short desorption times, indicating the reversibility of carmustine adsorption on the fullerene surfaces.

Natural Bond Orbital Analysis (NBO) are carried out to elucidate the bonding interactions anchoring Carm to both pristine B40 and metal-encapsulated fullerenes (Mg@B40 and K@B40), as well as to quantify the accompanying charge transfer. In B-O bonds and B-Cl anchor bonds, electron donation occurs from the O and Cl lone-pair orbitals into the boron antibonding (n*) orbitals. Because the three lone pairs on oxygen are differently oriented relative to these n* orbitals, they participate in the complex to varying degrees.

In the Table 2, the ΔECT values between donor and acceptor orbitals in Carm complexes with B40 and metal-encapsulated are listed.

Table 2. NBO charge transfer features of Carm-fullerene complexes

Complexes	**Interaction**	**ΔE_{CT}**
Carm1/B40	nO61 →n*B_{26}	0.06
Carm2/B40	nCl57 →n*B10	0.21
Carm1/k@B40	nO61 →n*B_{26}	0.35
Carm2/k@B40	nCl57→n*B_{10}	0.09
Carm1/Mg@B40	nO_{61} →n*B_{26}	0.1
Carm2/Mg@B40	nCl57→n*B_{10}	0.28

Overall, complexes characterized by lower orbital interaction (second-order perturbation) energies exhibit minimal charge transfer and thus display a predominantly ionic bonding character between the nanocage and the Carm molecule. As can be seen in Table 2, in all Carm complexes with B40 and M@B40, the interaction nO →n*B and nCl →n*B participates in the stabilization interaction. The most pronounced nO→n*B charge-transfer interaction occurs in the Carm/K@B40 complex, with ΔE_{CT} values of 0.35kcal/mol. Additionally,the most pronounced nCl→n*B charge-transfer interaction occurs in the Carm2/Mg@B40 complex(ΔE_{CT} =0.28Kcal/mol)

4. Conclusion

In this study, the adsorption of the carmustine drug on pristine fullerene, as well as on fullerenes encapsulating magnesium (Mg) and potassium (K) atoms, was investigated using the Density Functional Theory (DFT) computational method to evaluate the potential of these systems as electronic sensors for detecting carmustine. The results indicate that structural modification of fullerene leads to an increase in adsorption energy, a decrease in the energy gap, and, consequently, an enhancement in electrical conductivity within the studied systems. This increase in conductivity enables the generation of an electrical signal, supporting the use of modified fullerenes as promising candidates for sensing applications aimed at detecting the carmustine drug. The study revealed that electrostatic interactions, characteristic of a surface physical adsorption process, were involved. However, recovery time calculations indicate that these interactions are essentially irreversible, which is a critically important factor in sensor development. Furthermore, calculations of the work function and its percentage change for the respective complexes suggest that the modified fullerenes can serve as Φ-type nanosensors for the detection of carmustine, an anticancer drug. Our computational findings demonstrate the strong potential of metalloborophenes as sensitive and selective electronic sensors for detecting anticancer drugs such as Carmustine. Future research could focus on experimental validation of these results and the practical fabrication of metalloborophene-based nanosensors. Moreover, by tuning the metal dopant or surface functionalization, the sensing capabilities can be extended toward a broader range of chemotherapeutic agents and biomedical targets. This outlook emphasizes the promising role of metalloborophenes in the development of next-generation biosensing and drug-monitoring technologies.

References

[1] A.B. Fleming, W.M. Saltzman, Pharmacokinetics of the carmustine implant. *Clin. Pharmacokinet.* 41 (2002) 403–419.

[2] K.I. Lin, C.C. Lin, S.M. Kuo, J.C. Lai, Y.Q. Wang, H.L. You, et al., Carnosic acid impedes cell growth and enhances anticancer effects of carmustine and lomustine in melanoma. *Biosci. Rep.* 38 (2018) BSR20180005.

[3] A. Jones, J. Millar, B. Millar, B. Powell, P. Selby, A. Winkley, et al., Enhanced anti-tumour activity of carmustine (BCNU) with tumour necrosis factor in vitro and in vivo. *Br. J. Cancer* 62 (1990) 776–780.

[4] E. Musielak, V. Krajka-Kuźniak, Lipidic and Inorganic Nanoparticles for Targeted Glioblastoma Multiforme Therapy: Advances and Strategies. *Micro* (2025) 2.

[5] Z.Z. Xiao, Z.F. Wang, T. Lan, W.H. Huang, Y.H. Zhao, C. Ma, et al., Carmustine as a supplementary therapeutic option for glioblastoma: a systematic review and meta-analysis. *Front. Neurol.* 11 (2020) 1036.

[6] H.R. Kim, J.K. Hong, Y. Kim, J.Y. Choi, HEBP2 affects sensitivity to cisplatin and BCNU but not to paclitaxel in MDA-MB-231 breast cancer cells. *Toxicol. Res.* 40 (2024) 561–569.

[7] U.E. Laila, Z.L. Zhao, H. Liu, Z.X. Xu, Aspirin in Cancer Therapy: Pharmacology and Nanotechnology Advances. *Int. J. Nanomedicine* (2025) 2327–2365.

[8] R.B. Weiss, B.F. Issell, The nitrosoureas: carmustine (BCNU) and lomustine (CCNU). *Cancer Treat. Rev.* 9 (1982) 313–330.

[9] D. Fewer, C.B. Wilson, E.B. Boldrey, K.J. Enot, M.R. Powell, The chemotherapy of brain tumors: clinical experience with carmustine (BCNU) and vincristine. *JAMA* 222 (1972) 549–552.

[10] R.L. Schilsky, M.E. Dolan, D. Bertucci, R.B. Ewesuedo, N.J. Vogelzang, S. Mani, et al., Phase I clinical and pharmacological study of O6-benzylguanine followed by carmustine in patients with advanced cancer. *Clin. Cancer Res.* 6 (2000) 3025–3031.

[11] S.A. Chowdhary, T. Ryken, H.B. Newton, Survival outcomes and safety of carmustine wafers in the treatment of high-grade gliomas: a meta-analysis. *J. Neurooncol.* 122 (2015) 367–382.

[12] J.C. Buckner, K.V. Ballman, J.C. Michalak, G.V. Burton, T.L. Cascino, P.J. Schomberg, et al., Phase III trial of carmustine and cisplatin compared with carmustine alone and standard radiation therapy in patients with glioblastoma multiforme. *J. Clin. Oncol.* 24 (2006) 3871–3879.

[13] A.A. Brandes, A. Tosoni, U. Basso, M. Reni, F. Valduga, S. Monfardini, et al., Second-line chemotherapy with irinotecan plus carmustine in glioblastoma recurrent or progressive after first-line temozolomide chemotherapy. *J. Clin. Oncol.* 22 (2004) 4779–4786.

[14] H.S. Friedman, J. Pluda, J.A. Quinn, R.B. Ewesuedo, L. Long, A.H. Friedman, et al., Phase I trial of carmustine plus O6-benzylguanine for patients with recurrent or progressive malignant glioma. *J. Clin. Oncol.* 18 (2000) 3522–3528.

[15] A. Mali, A. Bhanwase, Stability Indicating Stress Degradation Study of Carmustine by UV-Spectrophotometric Method. *Res. J. Pharm. Technol.* 17 (2024) 3055–3060.

[16] Y. Wang, R. Zhu, Y. Ni, S. Kokot, Competitive interactions of anti-carcinogens with serum albumin: A spectroscopic study of bendamustine and dexamethasone with the aid of chemometrics. *Spectrochim. Acta A Mol. Biomol. Spectrosc.* 123 (2014) 241–248.

[17] R.G. Steen, K. Kitagishi, K. Morgan, In vivo measurement of tumor blood oxygenation by near-infrared spectroscopy: immediate effects of pentobarbital overdose or carmustine treatment. *J. Neurooncol.* 22 (1994) 209–220.

[18] M.R. Poor Heravi, B. Azizi, E. Abdulkareem Mahmood, A.G. Ebadi, M.J. Ansari, S. Soleimani-Amiri, Molecular simulation of the paracetamol drug interaction with Pt-decorated BC3 graphene-like nanosheet. *Mol. Simul.* 48 (2022) 517–525.

[19] M. Mohammadi, F. Alirezapour, Thioindole adsorption as a biologically active anticancer over C20 fullerene in different reaction media using density functional theory. *Chem. Rev. Lett.* 7 (2024) 201–210.

[20] S. Esfahani, J. Akbari, S. Soleimani-Amiri, M. Mirzaei, A.G. Gol, Assessing the drug delivery of ibuprofen by the assistance of metal-doped graphenes: insights from density functional theory. *Diamond Relat. Mater.* 135 (2023) 109893.

[21] S. Esfahani, J. Akbari, S. Soleimani-Amiri, Adsorption of Ibuprofen by an Iron-doped Silicon Carbide Graphene monolayer: DFT exploration of drug delivery insights. *Int. J. Nano Dimens.* 15 (2024).

[22] A. Yadav, A. Taha, Y.A. Abdulsayed, S.M. Saeed, A Density Functional Theory (DFT) Study on Adsorption of a biological active ethionamide over the Surface of a Fe-decorated porphyrin system. *Chem. Rev. Lett.* 6 (2023) 128–138.

[23] B. Mohammadi, M.R. Jalali Sarvestani, A comparative computational investigation on amantadine adsorption on the surfaces of pristine, C-, Si-, and Ga-doped aluminum nitride nanosheets. *J. Chem. Lett.* 4 (2023) 66–70.

[24] (a) R. Ghiasi, A. Valizadeh, *Results Chem.* 5 (2023) 100768; (b) A.S. Hessen, N.M.A. Alsultany, H. Bahir, A.H. Adthab, S. Soleimani-Amiri, S. Ahmadi, et al., *J. Mol. Graph. Model.* 135 (2025) 108928; (c) S. Soleimani-Amiri, A. Khanmohammadi, E. Vessally, J. Makasana, S. Ballal, R. Panigrahi, et al., *Comput. Theor. Chem.* 1253 (2025) 115457; (d) E. Vessally, H. Imanov, S. Soleimani-Amiri, Z. Hossaini, S. Abdolmohammadi, Z. Azizi, et al., *Microchem. J.* 219 (2025) 115961.

[25] (a) M. Rahimi, R. Ghiasi, *J. Mol. Liq.* 265 (2018) 164–171; (b) F. Alirezapour, F.S. Tahami, K. Bamdad, A. Khanmohammadi, S. Soleimani-Amiri, *Phosphorus Sulfur Silicon Relat. Elem.* (2026); (c) N.S. Yapo, K.E. Adou, J. Ano, D.N. Nonh, K.B. Yao, *J. Chem. Lett.* 4 (2023) 95–102.

[26] (a) R. Ghiasi, M.Z. Fashami, *J. Theor. Comput. Chem.* 13 (2014) 1450041; (b) N. Mirderikvand, M. Mahboubi-Rabbani, *J. Chem. Technol.* 1 (2025) 47–51; (c) N. Mirderikvand, M. Mahboubi-Rabbani, *J. Chem. Technol.* 1 (2025) 90–95.

[27] (a) N. Sadeghi, R. Ghiasi, R. Fazaeli, S. Jamehbozorgi, *J. Appl. Spectrosc.* 83 (2017) 909–916; (b) P. Gholami Dastnaei, *J. Med. Med. Chem.* 1 (2025) 1–6; (c) S. Arabi, *J. Med. Med. Chem.* 1 (2025) 38–42.

[28] (a) M. Rezazadeh, R. Ghiasi, S. Jamehbozorgi, *J. Appl. Spectrosc.* 85 (2018) 526–534; (b) R. Ahmadi, *J. Med. Med. Chem.* 1 (2025) 100–105; (c) B. Mohammadi, M.R. Jalali Sarvestani, *J. Chem. Lett.* 4 (2023) 66–70.

[29] H.H. Pang, Y.C. Ke, N.S. Li, Y.T. Chen, C.Y. Huang, K.C. Wei, et al., A new lateral flow plasmonic biosensor based on gold-viral biomineralized nanozyme for on-site intracellular glutathione detection. *Biosens. Bioelectron.* 165 (2020) 112325.

[30] K.J.F. Carnevale, Nano-biosensors: Probing Intracellular Response to Nanoparticle Therapy. *Florida State Univ.* (2018).

[31] C.M. Chima, H. Louis, D. Charlie, A. Imojara, I. Benjamin, E.E. Uzowuru, et al., Molecular simulation of Cu, Ag, and Au-decorated Molybdenum doped graphene nanoflakes as biosensor for carmustine, an anticancer drug. *Mater. Sci. Semicond. Process.* 165 (2023) 107669.

[32] T. Yadollahi, R. Ghiasi, S. Baniyaghoob, Unveiling of interactions of ansa-titanocene dichloride and ansa-vanadocene dichloride anticancer drugs with B12N12 cage. *Inorg. Chem. Commun.* 173 (2025) 113896.

[33] R. Ghiasi, M. Nikbakht, H. Pasdar, Interactions of the potential antitumor agent vanadocene dichloride with C20 and M+@C20 (M= Li, Na, K) nano-cages: A DFT investigation. *Results Chem.* 9 (2024) 101659.

[34] R. Ghiasi, M. Nikbakht, A. Amiri, Understanding the interactions between anticancer active molecules Cp2TiCl2 and Cp2VCl2 and E@Al12 (E= C, Si) clusters. *Inorg. Chem. Commun.* 164 (2024) 112446.

[35] A. Solgi, R. Ghiasi, S. Baniyaghoob, PCM, ETS-NOCV, and CDA investigations of interactions of a Cycloplatinated Thiosemicarbazone with C20 nano-cage. *Int. J. Nano Dimens.* 14 (2023).

[36] R. Ghiasi, A. Valizadeh, Interaction of cisplatin anticancer drug with C20 bowl: DFT investigation. *Main Group Chem.* 21 (2022) 43–54.

[37] M. Shabani, R. Ghiasi, K. Zare, R. Fazaeli, Quantum chemical study of interaction between titanocene dichloride anticancer drug and Al12N12 nano-cluster. *Russ. J. Inorg. Chem.* 65 (2020) 1726–1734.

[38] H. Kaur, J. Kaur, R. Kumar, Comparative study of symmetrical and asymmetrical B40 molecular junctions. *J. Comput. Electron.* 21 (2022) 599–607.

[39] M.S. Mussavi, S. Hosseini, DFT study on the potential of M@B40 (M= Mg and K) metalloborospherenes as nanocarrier for 6-Thioguanine anticancer drug. *J. Mol. Liq.* 395 (2024) 123900.

[40] E. Shakerzadeh, Li@B40 and Na@B40 fullerenes serving as efficient carriers for anticancer nedaplatin drug: A quantum chemical study. *Comput. Theor. Chem.* 1202 (2021) 113339.

[41] E. Shakerzadeh, Efficient carriers for anticancer 5-fluorouracil drug based on the bare and M-encapsulated (M= Na and Ca) B40 fullerenes. *J. Mol. Liq.* 343 (2021) 116970.

[42] E. Shakerzadeh, Endohedral M@B40 (M= Na and Ca) metalloborospherenes as innovative potential carriers for chemotherapy melphalan drug. *Appl. Organomet. Chem.* 35 (2021) e6411.

[43] C. Xiao, K. Ma, G. Cai, X. Zhang, E. Vessally, Borophene as an electronic sensor for metronidazole drug: A computational study. *J. Mol. Graph. Model.* 96 (2020) 107539.

[44] Y. Yong, X. Su, Y. Kuang, X. Li, Z. Lu, B40 and M@B40 (MLi and Ba) fullerenes as potential molecular sensors for acetone detection. *J. Mol. Liq.* 264 (2018) 1–8.

[45] C. Li, W. Tang, V. Vahabi, Identification of sulfur gases by an B40 fullerene: A computational study. *Physica E* 120 (2020) 114038.

[46] H. Kaur, J. Kaur, R. Kumar, A review on all boron fullerene (B40): A promising material for sensing and device applications. *Mater. Today Proc.* 48 (2022) 1095–1102.

[47] A.N. Sukumar, P.D. Duraisamy, P.M. Paul S, P. Gopalan, A. Angamuthu, Pristine B40 fullerene as a potential gemcitabine drug carrier for anti-lung cancer properties. *J. Biomol. Struct. Dyn.* (2024) 1–14.

[48] R. Rahimi, M. Solimannejad, In silico study of B3O3 nanosheet as a disposable platform for sensing and delivery of carmustine anticancer drug. *J. Drug Deliv. Sci. Technol.* 87 (2023) 104828.
[49] Y. Ying, X. Zhang, Y. Liu, M. Xue, H. Li, Y. Long, Single molecule study of the weak biological interactions between p53 and DNA. *Acta Chim. Sin.* 71 (2013) 44.
[50] M. Wu, A. Kumar, Pt-decorated graphene-like AlN nanosheet as a biosensor for tioguanine drug: A computational study. *Comput. Theor. Chem.* 1189 (2020) 112976.
[51] S.A. Aal, DFT study of the therapeutic potential of borospherene and metalloborospherenes as a new drug-delivery system for the 5-fluorouracil anticancer drug. *J. Mol. Liq.* 360 (2022) 119457.
[52] N.S. Shrikrishna, R. Sharma, J. Sahoo, A. Kaushik, S. Gandhi, Navigating the landscape of optical biosensors. *Chem. Eng. J.* (2024) 151661.
[53] E. Shakerzadeh, E. Tahmasebi, L.V. Duong, M.T. Nguyen, Boron clusters in biomedical applications: A theoretical viewpoint. *Characteristics and Applications of Boron, IntechOpen* (2022).
[54] S. Hedström, B. Rudshteyn, S. Chaudhuri, V.S. Batista, Marcus Theory with Gaussian and ADF—a Tutorial. (2016).
[55] M.J. Frisch, et al., Gaussian 09, Revision D.01. *Gaussian, Inc.* (2009).
[56] A.D. Becke, Perspective: Fifty years of density-functional theory in chemical physics. *J. Chem. Phys.* 140 (2014).
[57] L. Ning, S. Jingling, S. Jinhai, L. Laishun, X. Xiaoyu, L. Meihong, et al., Study on the THz spectrum of methamphetamine. *Opt. Express* 13 (2005) 6750–6755.
[58] T. Lu, F. Chen, Multiwfn: A multifunctional wavefunction analyzer. *J. Comput. Chem.* 33 (2012) 580–592.
[59] A.E. Reed, L.A. Curtiss, F. Weinhold, Intermolecular interactions from a natural bond orbital, donor-acceptor viewpoint. *Chem. Rev.* 88 (1988) 899–926.
[60] A.E. Reed, F. Weinhold, Natural bond orbital analysis of near-Hartree–Fock water dimer. *J. Chem. Phys.* 78 (1983) 4066–4073.
[61] A.E. Reed, F. Weinhold, Natural localized molecular orbitals. *J. Chem. Phys.* 83 (1985) 1736–1740.
[62] N.A.M. Radzuan, A.B. Sulong, J. Sahari, A review of electrical conductivity models for conductive polymer composite. *Int. J. Hydrog. Energy* 42 (2017) 9262–9273.
[63] M. Eslami, A.A. Peyghan, DNA nucleobase interaction with graphene like BC3 nano-sheet based on density functional theory calculations. *Thin Solid Films* 589 (2015) 52–56.
[64] J. Beheshtian, A.A. Peyghan, Z. Bagheri, Theoretical investigation of C60 fullerene functionalization with tetrazine. *Comput. Theor. Chem.* 992 (2012) 164–167.
[65] O. Richardson, Electron emission from metals as a function of temperature. *Phys. Rev.* 23 (1924) 153.
[66] N.L. Hadipour, A.A. Peyghan, H. Soleymanabadi, Theoretical study on the Al-doped ZnO nanoclusters for CO chemical sensors. *J. Phys. Chem. C* 119 (2015) 6398–6404.